The role of spinodal region in the kinetics of lattice phase transitions

Anna Vainchtein *

Department of Mathematics, University of Pittsburgh, Pittsburgh, PA 15260, USA

Abstract

We consider a one-dimensional chain of phase-transforming springs with harmonic long-range interactions. The nearest-neighbor interactions are assumed to be trilinear, with a spinodal region separating two material phases. We derive the traveling wave solutions governing the motion of an isolated phase boundary through the chain and obtain the functional relation between the driving force and the velocity of a phase boundary which can be used as the closing kinetic relation for the classical continuum theory. We show that a sufficiently wide spinodal region substantially alters the phase boundary kinetics at low velocities and results in a richer solution structure, with phase boundaries emitting short-length lattice waves in both direction. Numerical simulations suggest that solutions of the Riemann problem for the discrete system converge to the obtained traveling waves near the phase boundary.

1 Introduction

A remarkable property of materials undergoing martensitic phase transitions is the hysteresis they exhibit under cyclic loading as a result of energy dissipation by propagating phase boundaries. Kinetics of phase boundaries is thus a key to understanding the main features of the hysteretic behavior. On the continuum level martensitic phase transitions are modeled by a mixed-type hyperbolic-elliptic partial differential equation, and phase boundaries are represented as moving discontinuities of the deformation gradient. Since martensitic phase boundaries are typically subsonic, the resulting initial-value problem is ill-posed unless a closing *kinetic relation* (Slemrod, 1983; Truskinovsky, 1985) is specified in addition to the usual Rankine-Hugoniot jump conditions and dissipation inequality. Classical continuum elasticity provides no information

* Corresponding author
Email address: aav4@pitt.edu (Anna Vainchtein).

about this relation due to its failure to describe the internal structure of a phase boundary.

A recently proposed approach is to extract the kinetic relation from the underlying lattice model (Truskinovsky and Vainchtein, 2005a,b; Slepyan et al., 2005; Truskinovsky and Vainchtein, 2008; Purohit, 2002). The idea follows the earlier work in dislocation theory (Atkinson and Cabrera, 1965; Celli and Flytzanis, 1970; Ishioka, 1971; Kresse and Truskinovsky, 2004) and fracture (Slepyan and Troyankina, 1984; Slepyan, 1981; Marder and Gross, 1995). The discrete model provides the fine structure of the transition front that was eliminated in the continuum theory and thus resolves the ambiguity at the macroscale. To account for the macroscopic dissipation, one considers the traveling wave solutions that describe the motion of an isolated phase boundary. These solutions show that a moving interface emits short-length lattice waves which carry energy away from the propagating front. This radiative damping is perceived on the macroscopic level as energy dissipation. Accounting for the energy fluxes carried by the lattice waves, one can obtain the kinetic relation which can be used to supplement the continuum theory (Truskinovsky and Vainchtein, 2005b). The kinetic relation is commonly represented as the functional relation between the driving (configurational) force on a phase boundary and its velocity.

As shown by Truskinovsky and Vainchtein (2005b) and Slepyan et al. (2005), explicit solutions of the discrete problem can be found if one considers a one-dimensional lattice with bilinear interaction force between nearest neighbors (NN), which can be supplemented by harmonic long-range interactions (Truskinovsky and Vainchtein, 2005b). In this model, the NN force is linear in each phase and discontinuous at some critical strain which separates the two phases. The piecewise linearity allows one to construct traveling wave solutions using Fourier transform techniques and leads to a simple analytical expression for the kinetic relation. However, it neglects the *spinodal region*, the set of strains where the macroscopic elastic energy is nonconvex, which is represented by a single point of force discontinuity in the bilinear model.

In this paper we investigate the role of spinodal region in the kinetics of phase transitions. To do this, we consider a trilinear up-down-up NN interaction force, with spinodal region represented by the decreasing segment that can vary in width. Following Truskinovsky and Vainchtein (2005b, 2008), we also consider harmonic long-range interactions with an arbitary number of neighbors. To solve the problem with trilinear interactions, we adopt the approach of Flytzanis et al. (1977) which was proposed in the context of a screw dislocation motion but can be applied to other discrete problems that have a similar structure. Specifically, we express the strain in each NN spring in terms of an unknown shape function whose support determines the number of springs in the spinodal region. The shape function is then shown to be an eigenfunction

of a certain integral operator, and the corresponding eigenvalue is the width of the spinodal region. The kernel of the integral operator is determined by the solution of the bilinear problem, which is already explicitly known. Once the shape function is determined from the numerical solution of the eigenvalue problem, one can find the traveling wave solutions and the corresponding kinetic relation.

As in the work of Flytzanis et al. (1977), we find that the main effects of spinodal region are the phase shift and decreased amplitude of the emitted lattice waves and the lower value of the driving force. The differences are small at near-sonic velocities, suggesting that the bilinear model is adequate in that regime. However, a sufficiently wide spinodal region results in striking differences at small velocities which were not considered by Flytzanis et al. (1977). In particular, in the bilinear model and in the trilinear model with a narrow spinodal region there are no traveling wave solutions in some small-velocity intervals (velocity gaps). Meanwhile, a sufficiently wide spinodal region results in existence of traveling waves at many of these velocities and significantly narrows the velocity gaps. As a consequence, we obtain a richer solution structure, with phase boundaries emitting lattice waves of different frequencies in both directions, and a more complex kinetic relation that consists of several segments separated by the velocity gaps.

To verify the obtained solutions and check their stability, we conducted a series of numerical simulations of the Riemann problem for the discrete problem with an piecewise constant initial condition that has a single phase boundary. The strain in front of the phase boundary is fixed while the strain behind is varied and serves as a loading parameter. At small values of the applied strain the phase boundary is trapped. Once the strain exceeds a certain threshold, the phase boundary starts moving with some nonzero speed, and the solution around the phase boundary approaches the traveling wave solution with the corresponding velocity and driving force. As we continue increasing the applied strain, the numerical kinetic relation follows the one obtained from the traveling wave solutions and only involves phase boundary velocities for which there exists a traveling wave. Thus the numerically generated kinetic relation also has velocity gaps, suggesting that a phase boundary cannot move with certain velocities. Such velocity gaps are easy to miss in a numerical simulation, and a continuous kinetic curve interpolating the numerically computed points is assumed instead (Purohit, 2002).

This paper is organized as follows. In Section 2 we introduce the lattice model and derive the governing equations. Traveling wave solutions that model the motion of an isolated phase boundary are obtained in Section 3, and the kinetic relation is derived in Section 4. The results are presented in Section 5 and are compared to the numerical simulations in Section 6. Concluding remarks can be found in Section 7.

2 Lattice model

Consider a chain of particles, each interacting with its q neighbors on each side. Let $u_n(t)$ be the displacement of the nth particle. Then the total energy of the chain can be written as

$$\mathcal{E} = \varepsilon \sum_{n=-\infty}^{\infty} \left[\frac{\rho \dot{u}_n^2}{2} + \sum_{p=1}^{q} p\phi_p\left(\frac{u_{n+p} - u_n}{p\varepsilon} \right) \right], \tag{1}$$

where ε is the reference interparticle distance, ρ is the mass density per unit length, and $\phi_p(w)$ is the energy density of the interaction between pth nearest neighbors. The dynamics of the chain with energy (1) is governed by an infinite system of ordinary differential equations:

$$\rho \ddot{u}_n = \frac{1}{\varepsilon} \sum_{p=1}^{q} \left[\phi_p'\left(\frac{u_{n+p} - u_n}{p\varepsilon} \right) - \phi_p'\left(\frac{u_n - u_{n-p}}{p\varepsilon} \right) \right]. \tag{2}$$

These equations are the discrete analog of the partial differential equation

$$\rho u_{tt} = (\sigma(u_x))_x \tag{3}$$

governing the displacement $u(x,t)$ of a one-dimensional elastic bar with the macroscopic stress-strain relation

$$\sigma(w) = \sum_{p=1}^{q} p\phi_p'(w). \tag{4}$$

To obtain analytical results, we consider the simplest potentials that allow for a possibility of a phase transitions while capturing the essential features of the material behavior. We assume that the nearest-neighbor (NN) interactions are governed by a trilinear up-down-up interaction force:

$$\phi_1'(w) = \begin{cases} \mu_1 w, & w < w_c - \delta/2 \\ a\mu_1 \left(\dfrac{(\delta - a)w + w_c}{\delta} - \dfrac{1}{2} \right), & w_c - \delta/2 \le w \le w_c + \delta/2 \\ \mu_1 (w - a), & w > w_c + \delta/2, \end{cases} \tag{5}$$

where we assume that $0 < \delta < a$. See Fig. 1. The two linear segments $w < w_c - \delta/2$ and $w > w_c + \delta/2$ represent two different material phases; for simplicity, we assume that the elastic modulus $\mu_1 > 0$ is the same in both phases. The two phase regions are connected by the spinodal region $|w - w_c| < \delta/2$, where $\phi_1'(w) < 0$ when $\delta < a$, as assumed. Parameter δ thus measures the width of the spinodal region. When $\delta = 0$, we recover the bilinear interaction force with degenerate spinodal region studied by Truskinovsky and Vainchtein (2005b). In this case the phase switch occurs at $w = w_c$. The transformation strain

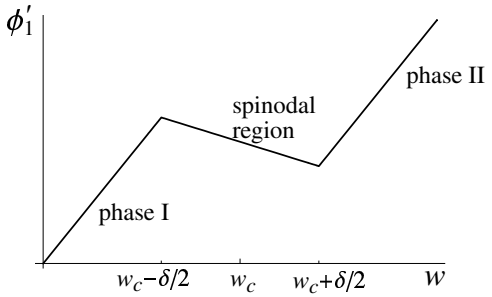

Fig. 1. The trilinear interaction force $\phi_1'(w)$ between the nearest neighbors

$a > 0$ is independent of w_c and δ and measures the distance between the two linearly increasing segments of $\phi_1'(w)$.

We further assume that the long-range interaction forces are linear:

$$\phi_p'(w) = p\mu_p w, \quad p = 2, ..., q. \tag{6}$$

It is convenient to reformulate the problem using dimensionless variables:

$$\begin{gathered} \bar{t} = t(\mu_1/\rho)^{1/2}/\varepsilon, \quad \bar{u}_n = u_n/(a\varepsilon), \quad \bar{w}_c = w_c/a, \quad \bar{\delta} = \delta/a, \\ \bar{\mu}_p = \mu_p/\mu_1, \quad p = 1, \ldots, q \quad (\bar{\mu}_1 = 1) \end{gathered} \tag{7}$$

Dropping the bars on the new variables and introducing the strain variables $w_n = u_n - u_{n-1}$, we can rewrite the governing equations (2) in the form

$$\ddot{w}_n = \sum_{p=2}^{q} \mu_p(w_{n+p} - 2w_n + w_{n-p}) + \phi_1'(w_{n+1}) - 2\phi_1'(w_n) + \phi_1'(w_{n-1}). \tag{8}$$

The macroscopic stress-strain relation (4) is the trilinear function

$$\sigma(w) = \begin{cases} c^2 w, & w < w_c - \delta/2 \\ \dfrac{(c^2\delta - 1)w + w_c}{\delta} - \dfrac{1}{2}, & w_c - \delta/2 \le w \le w_c + \delta/2 \\ c^2 w - 1, & w > w_c + \delta/2. \end{cases} \tag{9}$$

where

$$c = \left(\sum_{p=1}^{q} p^2 \mu_p \right)^{1/2} \tag{10}$$

is the dimensionless macroscopic sound speed in each phase. The microscopic elastic moduli μ_p must be chosen to ensure stability of the uniform deformation $w_n = w$ in each phase. For this it is necessary and sufficient that

$$\omega^2(k) = 4 \sum_{p=1}^{q} \mu_p \sin^2 \frac{pk}{2} > 0 \tag{11}$$

for $k \in (0, \pi]$. This implies, in particular, that the square c^2 of the macroscopic sound speed (10) must be positive. We will also assume that the long-range interactions, when included, have negative moduli ($\mu_p < 0$ for $p = 2, \ldots, q$), which is consistent with the linearization of the potentials of the Lennard-Jones type (Truskinovsky and Vainchtein, 2003, 2004) and penalizes formation of multiple phase boundaries. Note that the stability condition is satisfied, provided that the moduli are sufficiently small. The limits on the rescaled parameter δ ensuring the negative slope in the spinodal region for NN springs are now

$$0 < \delta < 1. \tag{12}$$

3 Traveling waves

Consider an isolated phase boundary moving with a constant velocity $V > 0$. It can be represented by a traveling wave solution of (8) with

$$w_n(t) = w(\xi), \quad \xi = n - Vt, \tag{13}$$

We assume the existence of a transition region $(-z, z)$ around the phase boundary, so that in the moving coordinate system all NN springs in the transition region ($|\xi| < z$) have strains in the spinodal part of the interaction potential: $|w(\xi) - w_c| < \delta/2$. Meanwhile, the NN springs behind and in front of the transition region are in high-strain and low-strain phases, respectively: $w(\xi) > w_c + \delta/2$ for $\xi < -z$ (phase II) and $w(\xi) > w_c - \delta/2$ for $\xi > z$ (phase I). Following Flytzanis et al. (1977), we write

$$\phi_1'(w(\xi)) = w(\xi) - \int_{-z}^{z} h(s)\theta(s - \xi)ds, \tag{14}$$

where $\theta(x)$ is the unit step function, and we introduced an unknown shape function $h(s)$ which is zero outside the interval $[-z, z]$ and is normalized so that

$$\int_{-z}^{z} h(s)ds = 1 \tag{15}$$

One can see that the normalization ensures that the NN springs belong to the proper phases outside the transition region. Note also that in the case $\delta = 0$ we have $z = 0$ and the shape function reduces to the Dirac delta function: $h(x) = \delta_0(x)$.

Using (13) and (14), we can replace the system (8) by a single nonlinear

advance-delay differential equation:

$$V^2 w'' - \sum_{p=1}^{q} \mu_p (w(\xi+p) - 2w(\xi) + w(\xi-p)) = \\ - \int_{-z}^{z} h(s)[\theta(s-\xi-1) - 2\theta(s-\xi) + \theta(s-\xi+1)]ds \tag{16}$$

The equation involves two unknown functions, $w(\xi)$ and $h(\xi)$, and the unknown half-width z of the transition region. Below we will follow the procedure outlined by Flytzanis et al. (1977) to derive an eigenvalue problem that will yield $h(\xi)$ and z. The configurations at $\xi = \pm\infty$ must correspond to stable homogeneous equilibria plus superimposed short-wave oscillations with zero average:

$$\langle w(\xi) \rangle \to w_{\pm}, \quad \text{as } \xi \to \pm\infty. \tag{17}$$

For consistency, we also need to require that

$$w(-z) = w_c - \delta/2, \quad w(z) = w_c + \delta/2 \tag{18}$$

and that the strains $w(\xi)$ remain in their respective phases, as assumed above.

Applying Fourier transform to the equation (16) (see Truskinovsky and Vainchtein (2005b) for details), we obtain

$$w(\xi) = w_- - \frac{2}{\pi i} \int_{\Gamma} \frac{\sin^2(k/2) H(k) e^{ik\xi} dk}{kL(k,V)}, \tag{19}$$

where

$$H(k) = \int_{-z}^{z} h(\xi) e^{-ik\xi} d\xi \tag{20}$$

is the Fourier transform of $h(\xi)$ (recall that $h(\xi) \equiv 0$ for $|\xi| > z$),

$$L(k,V) = 4 \sum_{p=1}^{q} \mu_p \sin^2 \frac{pk}{2} - V^2 k^2, \tag{21}$$

and the contour of integration Γ is chosen to properly resolve the singularities along the real axis. Specifically, the contour Γ coincides with the real axis everywhere except near the real roots of $L(k,V)$. It passes below the pole $k = 0$ and below the nonzero real roots of $L(k,V)$ if $kL_k(k,V) > 0$ and above if $kL_k(k,V) < 0$. As explained by Truskinovsky and Vainchtein (2005b), this ensures that our solution complies with the radiation condition that requires that oscillatory modes with group velocity $V_g = V + L_k(k,V)/(2Vk)$ larger than V can appear only in front, while the modes with $V_g < V$ can appear only behind the phase boundary (Slepyan, 2002).

In the case $z = 0$ ($\delta = 0$), we have $H(k) = 1$, and (19) reduces to the

corresponding expression for the strain $w^0(\xi)$ in the bilinear case:

$$w^0(\xi) = w^0_- - \frac{2}{\pi i}\int_\Gamma \frac{\sin^2(k/2)e^{ik\xi}dk}{kL(k,V)}. \tag{22}$$

Applying the residue theorem along with Jordan's lemma to (22) and enforcing the phase switch condition (18), which in this case reduces to $w(0) = w_c$, we obtain (Truskinovsky and Vainchtein, 2005b)

$$w^0(\xi) = \begin{cases} w^0_- + \sum\limits_{k\in M^-(V)} \dfrac{4\sin^2(k/2)e^{ik\xi}}{kL_k(k,V)}, & \xi < 0 \\ w^0_+ - \sum\limits_{k\in M^+(V)} \dfrac{4\sin^2(k/2)e^{ik\xi}}{kL_k(k,V)}, & \xi > 0, \end{cases} \tag{23}$$

where the average strains at infinity are determined by V via

$$w^0_\pm = w_c \mp \frac{1}{2(c^2-V^2)} + \sum_{k\in N_{\rm pos}(V)} \frac{4\sin^2(k/2)}{|kL_k(k,V)|}; \tag{24}$$

note that

$$w^0_+ = w^0_- - \frac{1}{c^2-V^2}. \tag{25}$$

Here

$$M^\pm(V) = \{k : L(k,V) = 0,\ {\rm Im}k \gtrless 0\} \bigcup N^\pm(V) \tag{26}$$

are all roots of the dispersion relation contributing to the solution on either side of the front, with

$$N^\pm(V) = \{k : L(k,V) = 0,\ {\rm Im}k = 0,\ kL_k(k,V) \gtrless 0\} \tag{27}$$

denoting the sets of real roots distributed according to the radiation condition, and in (24) the sum is over the set $N_{\rm pos}(V) = \{k : L(k,V) = 0,\ {\rm Im}k = 0, k > 0\}$ of all positive real roots of the dispersion relation.

To obtain z and $h(\xi)$ in the case of nonzero δ, observe that on one hand, (19) and (20) yield

$$\frac{dw}{d\xi} = -\int_{-z}^{z} h(s)q(\xi - s)ds, \tag{28}$$

where

$$\begin{aligned} q(\xi) =& \frac{2}{\pi}\int_\Gamma \frac{\sin^2(k/2)e^{ik\xi}dk}{L(k,V)} = -\frac{dw^0}{d\xi} \\ =& \begin{cases} -4i \sum\limits_{k\in M^-(V)} \dfrac{\sin^2(k/2)e^{ik\xi}}{L_k(k,V)}, & \xi < 0 \\ 4i \sum\limits_{k\in M^+(V)} \dfrac{\sin^2(k/2)e^{ik\xi}}{L_k(k,V)}, & \xi > 0. \end{cases} \end{aligned} \tag{29}$$

On the other hand, (14) and the rescaled version of (5) imply that for $|\xi| < z$

$$\frac{d}{d\xi}\phi_1'(w(\xi)) = \frac{\delta - 1}{\delta}\frac{dw}{d\xi} = \frac{dw}{d\xi} + h(\xi),$$

so that

$$\frac{dw}{d\xi} = -\delta h(\xi), \quad |\xi| < z.$$

Combining this with (28), we obtain the integral equation

$$\int_{-z}^{z} h(s)q(\xi - s)ds = \delta h(\xi), \quad |\xi| < z. \tag{30}$$

Thus the shape function $h(\xi)$ is the eigenfunction of the integral operator in the left hand side of (30) with the kernel (29) associated with the eigenvalue δ. The eigenvalue problem is similar to the the one obtained by Flytzanis et al. (1977) for the uniform motion of a screw dislocation (where the kernel is different) and was derived in the same way. For given $\delta > 0$ we can find z for which δ is the eigenvalue of the integral operator, with the corresponding eigenfunction.

Once z and $h(\xi)$ are known, we can find $w(\xi)$. Using (19) and (22), one can write the solution for the trilinear case as the convolution of the shape function and the solution (23) for $\delta = 0$ (bilinear NN interactions) which has already been found above in an explicit form. We obtain

$$w(\xi) = w_- - w_-^0 + \int_{-z}^{z} h(s)w^0(\xi - s)ds, \tag{31}$$

where we have also used (15). Applying the conditions (18), we can find the constant w_-:

$$w_- = w_c + w_-^0 - \frac{1}{2}\int_{-z}^{z} h(s)(w^0(z - s) + w^0(-z - s))ds. \tag{32}$$

Note that (31) along with (15) and (25) imply that

$$w_+ = w_- - \frac{1}{c^2 - V^2}, \tag{33}$$

which coincides with one of the Rankine-Hugoniot jump conditions. One can recover the second jump condition by computing particle velocities as in Truskinovsky and Vainchtein (2005b).

After the solution is constructed for given V and δ, we still need to verify that

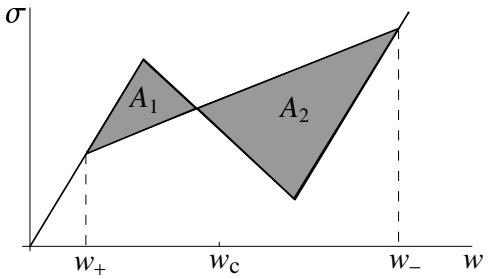

Fig. 2. The trilinear macroscopic stress-strain law and the Rayleigh line connecting the states at infinity for a traveling wave solution describing an isolated phase boundary. The difference between the shaded areas $A_2 - A_1$ equals the driving force.

it satisfies the assumed inequalities

$$\begin{aligned} &w(\xi) > w_c + \frac{\delta}{2}, \quad \xi < -z \\ &w_c - \frac{\delta}{2} < w(\xi) < w_c + \frac{\delta}{2}, \quad |\xi| < z \\ &w(\xi) < w_c - \frac{\delta}{2}, \quad \xi > z. \end{aligned} \tag{34}$$

Formally constructed solutions that violate these constraints are considered inadmissible and need to be discarded. This leads to non-existence of traveling wave solutions in certain intervals of low velocities. As we shall see, these intervals of non-existence become smaller as δ is increased.

4 Kinetic relation

The driving force on the phase boundary equals the difference between the shaded areas shown in Fig. 2. For the trilinear material at hand, it reduces to

$$G = \frac{w_+ + w_-}{2} - w_c. \tag{35}$$

Substituting (32), (33) and recalling (24), we obtain the kinetic relation

$$G(V;\delta) = G^0(V) + w_c - \frac{1}{2}\int_{-z}^{z} h(s)(w^0(z-s) + w^0(-z-s))ds, \tag{36}$$

where

$$G^0(V) = \sum_{k \in N_{\rm pos}(V)} \frac{4\sin^2(k/2)}{|kL_k(k,V)|} \tag{37}$$

is the kinetic relation obtained by Truskinovsky and Vainchtein (2005b) for $\delta = 0$. As δ tends to zero in (36), the integral in the last term tends to w_c, so that $G(V) \to G(V;0) \equiv G^0(V)$. Taking advantage of the explicit formula

(23) for $w^0(\xi)$, we can rewrite (36) in terms of residues of the integrand of (19) evaluated at the roots of the dispersion relation, obtaining

$$G(V;\delta) = \frac{1}{2}\left(\sum_{k\in M^+(V)} \frac{4\sin^2(k/2)}{kL_k(k,V)} H(k) e^{ikz} - \sum_{k\in M^-(V)} \frac{4\sin^2(k/2)}{kL_k(k,V)} H(k) e^{-ikz} \right), \tag{38}$$

where we recall that $H(k)$ is the Fourier transform of $h(\xi)$ defined in (20). For given V and δ, the roots of (21) (which are independent of δ), z and $H(k)$ can be found, and the right hand side of (38) thus furnishes a function of V and δ. At $\delta = 0$ we have $H(k) = 1$ and $z = 0$, so that due to the symmetry of the non-real roots (if $k \in M^+(V)\backslash N^+(V)$, then $-k \in M^-(V)\backslash N^-(V)$) and the fact that the expression under the sum is even in this case, the summations over the non-real roots cancel out, and we recover (37).

5 Results

To keep things simple, we now consider the case $q = 2$: nearest and next-to-nearest neighbor (NNN) interactions only. In this case it is convenient to use the parameter $\beta = 4\mu_2/\mu_1$ measuring the relative strength of NNN interactions, and our assumptions on the elastic moduli reduce to

$$-1 < \beta < 0,$$

with $c^2 = 1 + \beta$. The structure of the roots of the dispersion relation (21) for this case and its effect on the traveling wave solutions (23) and kinetic relation (37) for bilinear NN interactions have been extensively studied by Truskinovsky and Vainchtein (2005b), where the role of β was analyzed (see also Truskinovsky and Vainchtein, 2008). NNN interactions with negative β serve as a discrete analog of the interfacial energy term in continuum models, penalizing the formation of new interfaces and providing an internal structure of a phase boundary even in the static case (Truskinovsky and Vainchtein, 2004). In this paper we fix β and focus our attention on the role of the parameter δ which measures the width of the spinodal region.

We first review some basic features of the solutions in the bilinear case $\delta = 0$. There exist infinitely many *resonance velocities* V_i, $V_{i+1} < V_i < V_0 \equiv c$, where $L_k(k, V_i) = 0$ and thus the solution (23) blows up. For V between the resonance values, the traveling wave solution exhibits oscillations which correspond to phonons emitted by a moving phase boundary. According to the radiation condition, the oscillation modes with $k \in N^+(V)$ appear in front ($\xi > 0$), and the modes with $k \in N^-(V)$ are behind the moving front ($\xi < 0$). It can be shown that the number of modes appearing behind is always larger by one. For velocities V such that $V_1 < V < c$ we have only a single oscillation

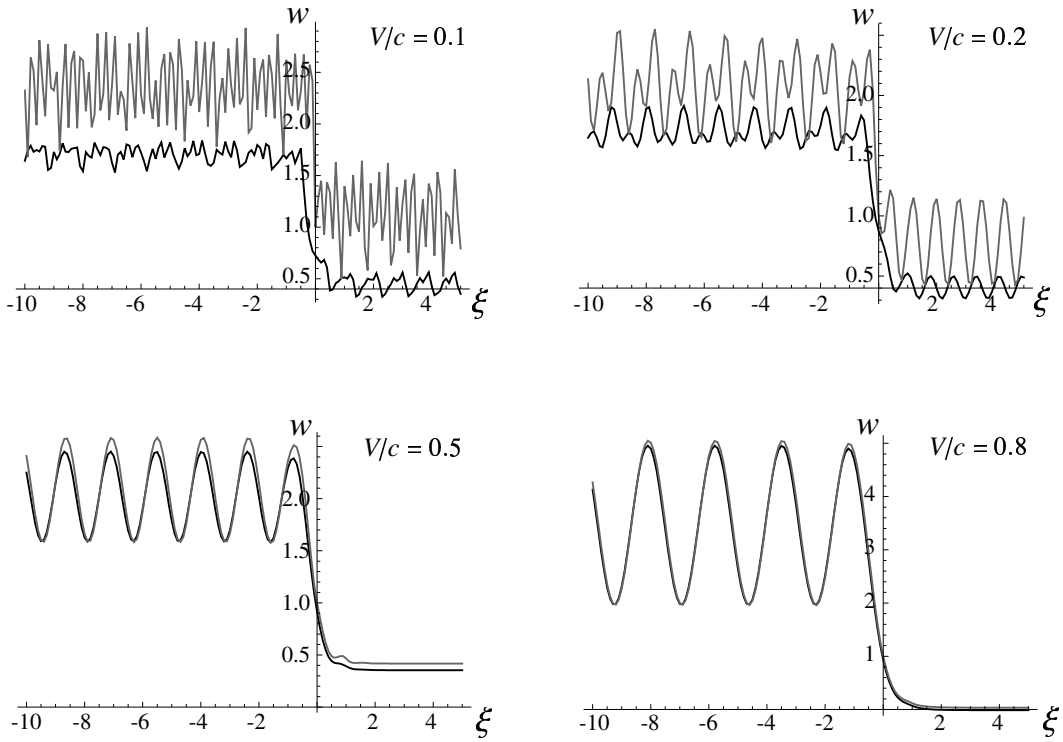

Fig. 3. Strain profiles at various velocities of the phase boundary. The grey curves are solutions for the bilinear case ($\delta = 0$), and the black curves are solutions at $\delta = 0.8$. Other parameters: $w_c = 1$, $\beta = -0.2$.

mode behind and no oscillations in front. For $V \in (V_2, V_1)$ and lower velocity intervals there are oscillations both behind and in front. See the grey curves in Fig. 3. However, as discussed in Truskinovsky and Vainchtein (2005b), not all of the solutions constructed using (23) are actually admissible, i.e. satisfy the constraints $w(\xi) > w_c$ for $\xi < 0$ and $w(\xi) < w_c$ for $\xi > 0$. Sufficiently large amplitude of oscillations results in the constraints being violated. At small enough β this means that no traveling wave solutions actually exist in the entire low-velocity region (Truskinovsky and Vainchtein, 2005b). For example, solutions in Fig. 3 at $\delta = 0$ (grey lines) are not admissible when $V/c = 0.1$ and 0.2.

To find solutions at nonzero δ, we first computed the solution (23) for the bilinear case along with the kernel (29). We then used the trapesoidal approximation of the integral in (30) for a finite z, so that the eigenvalue problem reduces to finding z and $\mathbf{h}$ such that the given δ is an eigenvalue of the resulting matrix in the numerical approximation, and the vector $\mathbf{h}$ is the corresponding eigenvector that approximates the eigenfunction $h(\xi)$. In some cases, there were two values of z but at most one value yielded admissible solutions that satisfied the constraints (34). Once z and $\mathbf{h}$ were found, we used the trapesoidal approximation of the integrals in (31) and (32) to compute the solution $w(\xi)$. For small values of δ (and hence z), it is possible to approximate the

kernel (29) by a linear or quadratic polynomial (Flytzanis et al., 1977) in the interval $(-z, z)$, and this yields analytical expressions for z and $h(\xi)$ which we used to verify numerically computed solutions and obtain the initial guess for the numerical root-finding procedure.

The main effects of $\delta > 0$ are the phase shift and decreased amplitude of the oscillations, as well as the lower value of the driving force, which means lower w_- (see Fig. 3). This was also observed and explained by Flytzanis et al. (1977) in the context of dislocation motion. The phase shift occurs due to the continuous particle acceleration at $\delta > 0$ (as opposed to the discontinuity at $t = n/V$ when $\delta = 0$), which results in lower velocities and thus longer time needed to reach the maxima of oscillations. Meanwhile, the decrease in both the amplitude of the oscillations and the driving force is due to the finite time interval $[(n - z)/V, (n + z)/V]$ during which the force-strain law in the phase-transforming nth spring has the negative slope, resulting in an interference of the emitted waves and leading to the smaller contribution of the short-wave oscillations to the energy radiation. These effects of nonzero δ are very pronounced at low velocities ($V/c < 0.5$), when z is larger.

As the consequence of this, non-resonance velocities for which there are no admissible traveling wave solutions in the bilinear case result in admissible solutions for sufficiently large δ. Consider, for example, solutions at $V/c = 0.1$ and $V/c = 0.2$ shown in Fig. 3. The strain profiles at $\delta = 0$ (grey curves) are clearly not admissible but both solutions become admissible at $\delta = 0.8$ (black curves). Indeed, due to the decreased amplitude of oscillations these solutions satisfy the constraints (34). Thus, as δ increases, the velocity intervals where traveling wave solutions exist become larger. Of course, due to the presence of resonances, there are still "velocity gaps" around the resonance speeds where there are no traveling wave solutions even at large δ but these gaps become narrower as δ increases. This implies that uniform phase boundary motion may occur at least at some low velocities in the trilinear case, while in the degenerate bilinear model this was only possible at unrealistically high values of β (Truskinovsky and Vainchtein, 2005b).

As V increases, z becomes smaller, as shown in Fig. 4b, and the difference from the bilinear case becomes less pronounced (see Fig. 3), so that at near-sonic speeds the solutions are very close. Thus the bilinear model provides an adequate approximation for the trilinear case at medium to high velocities, with the lower limit becoming higher at wider spinodal region. We remark, however, that at high velocities solutions are also well approximated by quasicontinuum models (Truskinovsky and Vainchtein, 2006, 2008), so the discrete model is primarily needed at lower velocities where the quasicontinuum models are no longer adequate.

Kinetic relations for $\delta = 0$ and $\delta = 0.8$ cases formally constructed from (36)

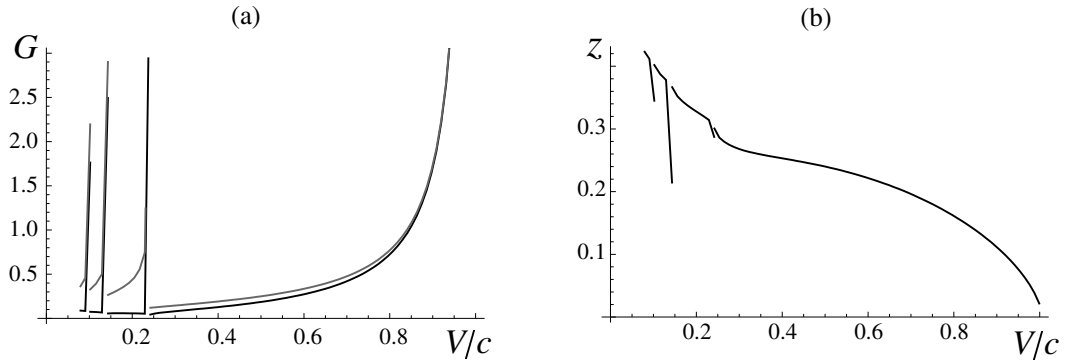

Fig. 4. (a) The kinetic relations at $\delta = 0$ (grey) and $\delta = 0.8$ (black). Only the first four segments are shown. In the bilinear case (the grey curves), the lower-velocity segments ($V < V_1$) do not contain admissible solutions and need to be excluded. In the trilinear model, the corresponding segments contain admissible solutions away from the resonance velocities (see the text for discussion). (b) The corresponding graph z versus V for the trilinear model. Other parameters: $\beta = -0.2$.

and (37) are shown in Fig. 4a. As discussed above, it consists of segments separated by the resonance velocities (only the first four segments are shown). In the bilinear case (the grey curves), all segments except the first (higher-velocity) one need to be removed because they do not contain admissible solutions, while in the case $\delta = 0.8$ low-velocity solutions away from the resonance velocities can become admissible, as shown in the above examples.

Lattice trapping and the Peierls threshold. In addition to the traveling wave solution with nonzero V, there are equilibrium solutions of (8) that correspond to a phase boundary trapped in the lattice. In particular, consider equilibria that have all NN springs behind the phase boundary in phase II and all springs in front in phase I, with no springs in the spinodal region. For a phase boundary located at $n = 0$ and $q = 2$ this yields (Truskinovsky and Vainchtein, 2003)

$$w_n = w_c + G + \begin{cases} \dfrac{1}{2(1+\beta)} - \dfrac{e^{\lambda(n-1/2)}}{2(1+\beta)\cosh(\lambda/2)}, & n \le 1 \\ -\dfrac{1}{2(1+\beta)} + \dfrac{e^{-\lambda(n-1/2)}}{2(1+\beta)\cosh(\lambda/2)}, & n \ge 0, \end{cases} \tag{39}$$

where $\lambda = 2\mathrm{arccosh}(1/\sqrt{-\beta})$ and the strains must satisfy

$$w_n \le w_c - \frac{\delta}{2}, \quad n \ge 1, \qquad w_n \ge w_c + \frac{\delta}{2}, \quad n \le 0.$$

This means that the driving force G compatible with such an equilibrium state must be inside the trapping region

$$|G| \le G_{\mathrm{P}}, \tag{40}$$

where $G_{\rm P}$ is the Peierls threshold given by

$$G_{\rm P} = \frac{1}{2\sqrt{1+\beta}} - \frac{\delta}{2}. \tag{41}$$

In general, the equilibrium states can have one or more springs in the spinodal region, and the expression for the corresponding Peierls stress depends on δ in a more complicated way (Weiner and Sanders, 1964).

6 Numerical solution of the Riemann problem and comparison with the semi-analytical results

To determine stability of the traveling wave solutions obtained above and explore the possible existence of other solutions that are not of traveling wave type, we performed numerical simulations of the Riemann problem. Specifically, we used the Verlet algorithm to solve the system (8) for the case $q = 2$ on a sufficiently large lattice (600 particles) with the following initial conditions for the NN strains w_n:

$$w_n(0) = \begin{cases} w_L, & n < n_0 \\ w_c, & n = n_0 \\ 0, & n > n_0, \end{cases} \tag{42}$$

where $s > w_c + \delta/2$ and we assume that $w_c - \delta/2 > 0$, so that NN springs in front of and behind $n = n_0$ (the center of the chain) are initially in phase I and II, respectively. The particle velocity is initially zero throughout the chain. The analysis of the corresponding continuum problem for the equation (3) suggests the propagation of a phase boundary with shocks in front and behind it (e.g. Ngan and Truskinovsky, 2002). This is indeed what we see in Fig. 5 showing a typical numerical solution of the Riemann problem. One can see that after an initial transient period the phase boundary propagates with a uniform velocity. To facilitate comparison with the analytical traveling wave solution that has $V/c = 0.2$, we applied the strain $w_L = 2.37472$ which yields the same driving force, assuming that the kinetic relation we derived from the traveling wave solution holds for the phase boundary in the numerical calculations. More specifically, using the Rankine-Hugoniot jump conditions with the initial conditions (42) and recalling that the initial particle velocity is zero, we obtain

$$w_L = 2G + w_c + \frac{V}{c(c^2 - V^2)}, \tag{43}$$

where we also used (35). For given V, we can use either (36) or (38) to compute the driving force G and thus determine the corresponding w_L. If the numerical solution obtained with this initial condition agrees with the traveling wave solution near the phase boundary, it should generate the same velocity of the

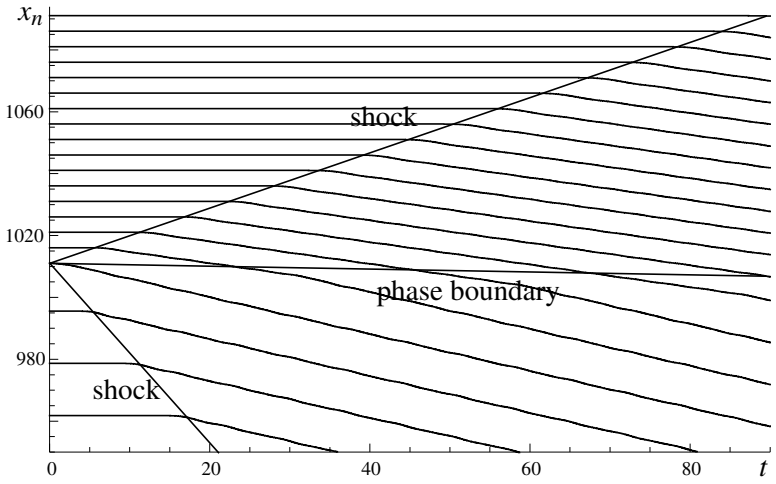

Fig. 5. Positions $x_n(t)$ of every fifth particle in the interval $280 \leq n \leq 380$ in numerical solution of the Riemann problem with the left strain $w_L = 2.37472$ in the initial data and the parameters $\beta = -0.2$, $\delta = 0.8$, $w_c = 1$. The phase boundary is initially placed at $n_0 = 300$, and the problem is solved on the interval $1 \leq n \leq 600$. The initial data was chosen to be compatible with the traveling wave solution with velocity $V = 0.2c$, and the numerical solution generates the same velocity of the phase boundary.

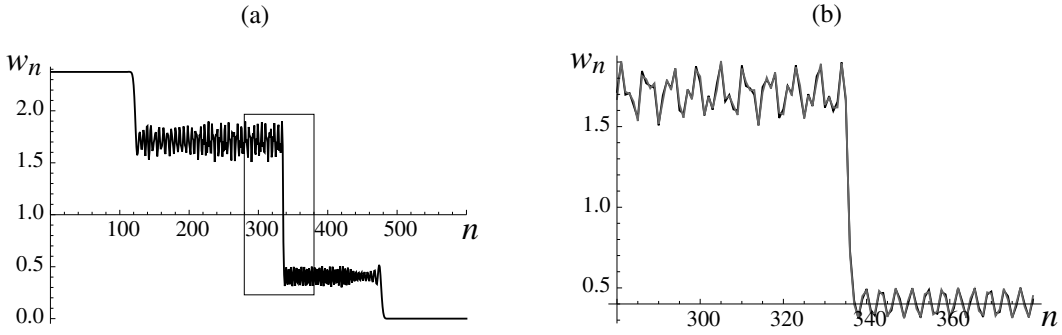

Fig. 6. (a) Strain profile $w_n(200)$ for the numerical solution shown in Fig. 5. (b) The same solution (black curve) zoomed in around the phase boundary (inside the rectangle in (a)) and compared to the analytical traveling wave solution (grey curve).

phase boundary propagation. This turns out to be the case for $V/c = 0.2$, as illustrated in Fig. 6. Part (a) of the figure shows the strain profile for the numerical solution at $t = 200$. In part (b) the same profile is zoomed around the phase boundary (the black curve) and compared to the appropriately shifted traveling wave solution (the grey curve). The agreement between the two solutions is remarkably good, suggesting stability of the traveling wave solution in this example.

To compare the numerical and analytical solutions across a wide range of velocities, we conducted the numerical simulations at different values of the

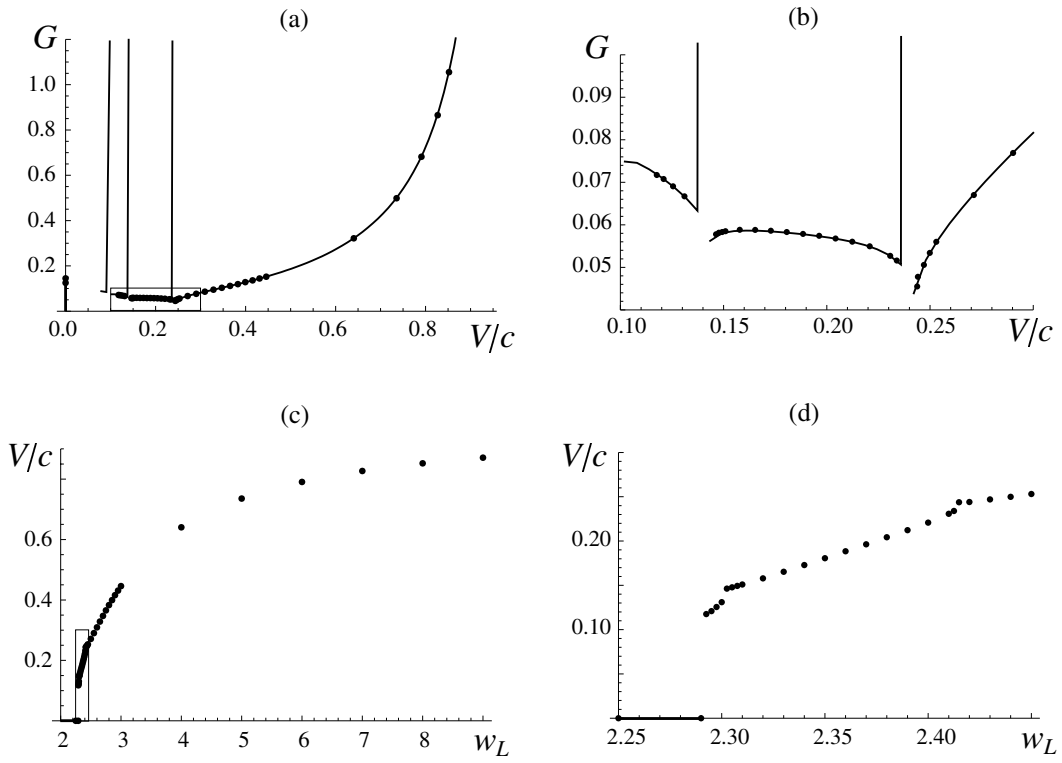

Fig. 7. (a) The first four segments of the kinetic relation $G(V)$ (solid lines) and the values obtained from the numerical simulation of the Riemann problem (dots). (b) Zoom-in of the rectangle in part (a). (c) Velocity V of the steady interface propagation as the function of the left strain w_L. (d) Zoom-in of the rectangle in part (c). Thick solid segments along $V = 0$ indicate the regions where the phase boundary in the numerical solution is trapped. Parameters: $\delta = 0.8$, $\beta = -0.2$.

left strain w_L and computed the resulting velocity V at large time (averaged over the last five periods) and the corresponding driving force

$$G = \frac{w_L}{2} - w_c - \frac{V}{c(c^2 - V^2)}$$

(recall (43)) for each initial condition. The results are shown in Fig. 7. Part (a) compares the numerical kinetic relation (dots) to the semi-analytical one (solid curves). Note that in this figure the portions of the semi-analytical kinetic relation where the traveling solutions are not admissible (around the resonances and at small enough velocities) have not been removed. Part (b) shows the small-velocity region in more detail. The graph of phase boundary velocity as the function of the left strain w_L is presented in part (c), and part (d) is the zoom-in of the same graph at small velocities. One can see that at sufficiently small w_L, corresponding to G below the Peierls threshold (41), the velocity of the phase boundary is zero. At $w_L = 2.2925$ (and $G = 0.1462$, which is still below the Peierls value $G_{\rm P} = 0.159$) the velocity jumps from zero to the value $V = 0.1175c$, with the driving force value on the third segment (counting from larger to smaller velocities) of kinetic curve we obtained using

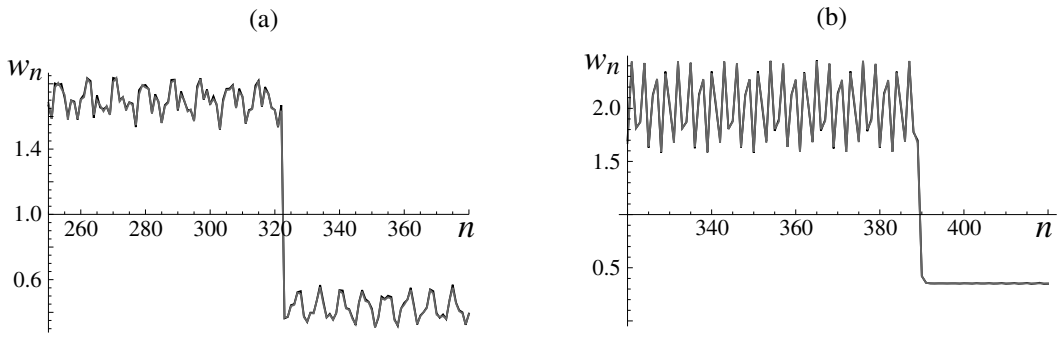

Fig. 8. Strain profiles of the numerical solution $w_n(200)$ zoomed around the phase boundary (black curve) and the traveling wave solution (grey curve) at (a) $V/c = 0.1255$ ($w_L = 2.2975$) and (b) $V/c = 0.5$ ($w_L = 3.20606$). In both cases the two solutions are very close, suggesting stability of the traveling wave solution. Parameters: $\delta = 0.8$, $\beta = -0.2$.

the traveling wave solution. As w_L increases, the velocity continues to increase, while the numerical kinetic relation follows this segment until the velocity reaches the value $V = 0.131c$, below the second resonance, at $w_L = 2.3$. At $w_L = 2.3025$, the velocity jumps to the value $V = 0.1463c$, which is above the second resonance, with the driving force close to the second segment of the semi-analytical kinetic relation. This segment is followed until $V = 0.2339c$ ($w_L = 2.4125$), below the first resonance, whereupon the velocity jumps again, to the value $V = 0.2438c$ ($w_L = 2.415$), and the numerical kinetic relation follows the first segment of the kinetic curve we obtained earlier. See parts (b) and (d) of Fig. 7 for details.

The simulation shows that at large time the numerical solutions converge to the corresponding admissible traveling wave solutions in the region around the phase boundary. In addition to the above example of $V/c = 0.2$ (Fig. 6) along the second kinetic segment, this is illustrated in Fig. 8 that depicts both solutions at $V/c = 0.1255$ (the third kinetic segment) and $V/c = 0.5$ (the first kinetic segment). This suggests stability of the admissible low-velocity traveling wave solutions with $V/c \geq 0.1175$, which have oscillations both behind and in front of the moving boundary. Recall that in the case $\delta = 0$ there are no admissible traveling wave solutions of this type.

An important feature of the numerical simulation is the presence of the *velocity gaps*, or discontinuities in the $V = V(s)$ graph. The first gap is between $V = 0$ and $V/c = 0.1175$. As described above, the phase boundary remains trapped at $n = n_0$ until the left strain reaches the value $w_L = 2.2925$. Each numerical solution with a trapped boundary is a superposition of the equilibrium state (39) around the phase boundary and the two shock waves moving away from it. Fig. 9 shows the solution at $w_L = 2.29$, just before the velocity jumps to a nonzero value. Note that the NN spring just in front of the phase boundary has not reached the spinodal region yet, so that the driving force, $G = 0.145$ is still

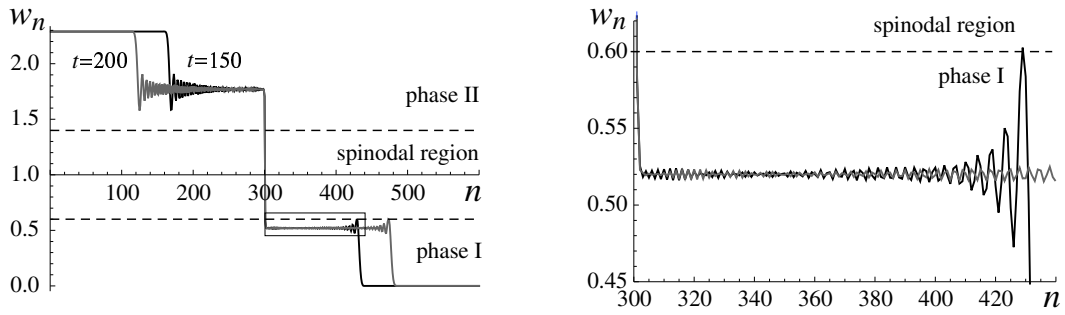

Fig. 9. (a) Strain profiles of the numerical solution $w_n(150)$ (black curve) and $w_n(200)$ (grey curve) at $w_L = 2.29$.(b) Zoom-in of the rectangle in part (a). The dashed lines indicate the boundaries of the spinodal region. Parameters: $\delta = 0.8$, $\beta = -0.2$.

below the Peierls threshold $G_{\rm P} = 0.159$. Observe, however, the characteristic "overshoot" oscillatory structure (Chin, 1975) behind the shock fronts. As one can see in Fig. 9b, at $w_L = 2.29$ the peak value of this structure behind the shock moving ahead of the phase boundary is already inside the spinodal region (although just barely). Equilibrium phase boundary at higher G (and thus higher w_L) results in higher average strain w_+ behind the shock (in front of the phase boundary), thus pushing the oscillation peak further inside the spinodal region and making the solution unstable. Instead, as we increase the left strain to $w_L = 2.2925$, the system approaches a state with nonzero velocity ($V = 0.1175c$) that has NN springs ahead and behind the phase boundary in their respective phases, including the springs behind the shock fronts.

The other two velocity gaps, V/c between 0.131 and 0.1463 and between 0.2339 and 0.2438, are around the resonance velocities. Interestingly, these gaps are the velocity intervals where there are no admissible traveling waves. Thus, the numerical solution only selects velocities for which there are admissible traveling waves and approaches the corresponding traveling wave solution in the region around the phase boundary.

To study the effect of δ, we also conducted the same numerical simulation at $\delta = 0.4$ and $\delta = 0$ (the bilinear case). The results are shown in Figs. 10 and 11. One can see that as δ decreases, the first nonzero velocity becomes higher, equal to $V = 0.2641c$ at $\delta = 0.4$ and $V = 0.3816c$ at $\delta = 0$. In both cases the numerical solution jumps to the first (highest velocities) segment, whereas at $\delta = 0.8$ we saw it jumping to $V = 0.1175c$ and following the third segment. As a result, a narrow spinodal region results in phase boundaries with oscillations behind and no waves emitted in front, while a sufficiently wide spinodal region (e.g. $\delta = 0.8$) yields a richer solution structure, with waves propagating both behind and in front of a phase boundary at smaller velocities, and a more complicated kinetic relation with two or more velocity gaps. One can also see that the bilinear model grossly overestimates the lowest nonzero speed of a

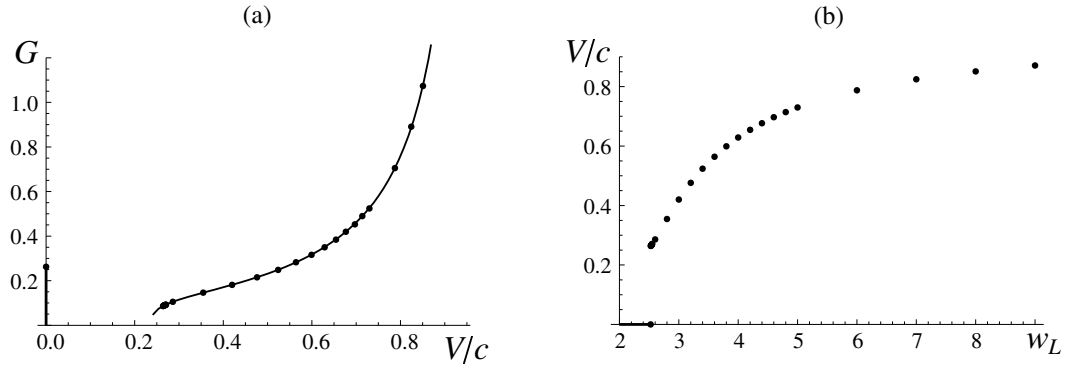

Fig. 10. (a) The first segment of the kinetic relation $G(V)$ (solid line) and the values obtained from the numerical simulation of the Riemann problem (dots). (b) Velocity V of the steady interface propagation as the function of the left strain w_L. Thick solid segments along $V = 0$ indicate the regions where the phase boundary in the numerical solution is trapped. Parameters: $\delta = 0.4$, $\beta = -0.2$.

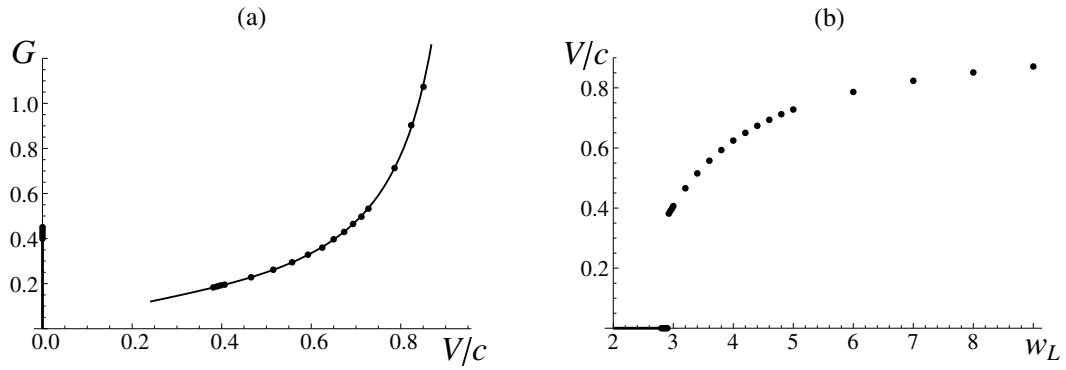

Fig. 11. (a) The first segment of the kinetic relation $G(V)$ (solid line) and the values obtained from the numerical simulation of the Riemann problem (dots). (b) Velocity V of the steady interface propagation as the function of the left strain w_L. Thick solid segments along $V = 0$ indicate the regions where the phase boundary in the numerical solution is trapped. Parameters: $\delta = 0$, $\beta = -0.2$.

phase boundary.

7 Conclusions

In this work we considered the effect of the spinodal region on the kinetics of martensitic phase transitions. Our results use and expand the previously obtained explicit solution for the bilinear model to solve the problem with trilinear NN interactions. This extension is nontrivial, as the problem can no longer be solved using only simple transform techniques and requires finding an eigenfunction of an integral operator, a method proposed by Flytzanis et al. (1977) for a discrete model of a screw dislocation. It also provides a

more realitic model of the actual material behavior by considering stress-strain curves with a non-degenerate spinodal region. We show that the effect of spinodal region is particularly important at small velocities where some traveling wave solutions that were inadmissible in the bilinear problem become admissible when the spinodal region is sufficiently wide due to the decreased amplitude of oscillations that in the bilinear case pushed the solution outside the assumed phase distribution. Interestingly, the inadmissible solutions of the bilinear problem still play an important role, as they provide the kernel for the integral equation which is used to obtain solutions for the trilinear case that may be admissible.

We show that a sufficiently wide spinodal region thus results in a richer structure of solutions, including low-velocity phase boundaries that emit lattice waves in both directions. Our numerical simulations suggest stability of these solutions starting with a certain minimum velocity that decreases as the spinodal region becomes wider. They also show that a phase boundary in the solution of the Riemann problem cannot move with velocities for which there is no traveling wave solution. This suggests that the kinetic relation obtained in this work, with inadmissible solutions removed, accurately describes the phase boundary kinetics for velocities above the minimum nonzero speed. As the spinodal region becomes wider, the kinetic relation includes more segments separated by the velocity gaps. The bilinear model provides a good approximation of phase boundary kinetics at near-sonic velocities but overestimates the minumum speed and the driving force at all velocities.

By providing an insight into the effects of an essential nonlinearity, our analysis contributes to the understanding of the complex dynamics of a phase boundary in a nonlinear chain. Clearly, the fully nonlinear problem also presents substantial additional challenges, such as mode mixing and subsequent thermalization. The work in this direction is currently under way.

Acknowledgements. This work was supported by the National Science Foundation grant DMS-0443928.

References

Atkinson, W., Cabrera, N., 1965. Motion of a Frenkel-Kontorova dislocation in a one-dimensional crystal. Physical Review A 138 (3), 763–766.

Celli, V., Flytzanis, N., 1970. Motion of a screw dislocation in a crystal. Journal of Applied Physics 41 (11), 4443–4447.

Chin, R. C. Y., 1975. Dispersion and Gibbs phenomenon associated with difference approximations to the initial boundary-value problems for hyperbolic equations. Journal of Computational Physics 18, 233–247.

Flytzanis, N., Crowley, S., Celli, V., 1977. High velocity dislocation motion and interatomic force law. J. Phys. Chem. Solids 38, 539–552.

Ishioka, S., 1971. Uniform motion of a screw dislocation in a lattice. J. Phys. Soc. Jpn. 30, 323–327.

Kresse, O., Truskinovsky, L., 2004. Lattice friction for crystalline defects: from dislocations to cracks. Journal of the Mechanics and Physics of Solids 52, 2521–2543.

Marder, M., Gross, S., 1995. Origin of crack tip instabilities. Journal of the Mechanics and Physics of Solids 43, 1–48.

Ngan, S.-C., Truskinovsky, L., 2002. Thermo-elastic aspects of dynamic nucleation. Journal of the Mechanics and Physics of Solids 50, 1193–1229.

Purohit, P. K., 2002. Dynamics of phase transitions in strings, beams and atomic chains. Ph.D. thesis, California Institute of Technology, Pasadena, California.

Slemrod, M., 1983. Admissibility criteria for propagating phase boundaries in a van der Waals fluid. Archive for Rational Mechanics and Analysis 81, 301–315.

Slepyan, L. I., 1981. Dynamics of a crack in a lattice. Soviet Physics Doklady 26 (5), 538–540.

Slepyan, L. I., 2002. Models and phenomena in Fracture Mechanics. Springer-Verlag, New York.

Slepyan, L. I., Cherkaev, A., Cherkaev, E., 2005. Transition waves in bistable structures. II. Analytical solution: wave speed and energy dissipation. Journal of the Mechanics and Physics of Solids 53, 407–436.

Slepyan, L. I., Troyankina, L. V., 1984. Fracture wave in a chain structure. Journal of Applied Mechanics and Technical Physics 25 (6), 921–927.

Truskinovsky, L., 1985. Structure of an isothermal phase jump. Soviet Physics Doklady 30, 945–948.

Truskinovsky, L., Vainchtein, A., 2003. Peierls-Nabarro landscape for martensitic phase transitions. Physical Review B 67, 172103.

Truskinovsky, L., Vainchtein, A., 2004. The origin of nucleation peak in transformational plasticity. Journal of the Mechanics and Physics of Solids 52, 1421–1446.

Truskinovsky, L., Vainchtein, A., 2005a. Explicit kinetic relation from "first principles". In: Steinmann, P., Maugin, G. (Eds.), Mechanics of Material Forces. Springer, pp. 43–50.

Truskinovsky, L., Vainchtein, A., 2005b. Kinetics of martensitic phase transitions: Lattice model. SIAM Journal on Applied Mathematics 66, 533–553.

Truskinovsky, L., Vainchtein, A., 2006. Quasicontinuum models of dynamic phase transitions. Continuum Mechanics and Thermodynamics 18 (1-2), 1–21.

Truskinovsky, L., Vainchtein, A., 2008. Dynamics of martensitic phase boundaries: discreteness, dissipation and inertia. Continuum Mechanics and Thermodynamics 20 (2), 97–122.

Weiner, J. H., Sanders, W. T., 1964. Peierls stress and creep in a linear chain.

Physical Review 134 (4A), 1007–1015.